

# On-the-fly Tailoring towards a Rational Ansatz Design for Digital Quantum Simulations

Dibyendu Mondal, Sonaldeep Halder, Dipanjali Halder, Rahul Maitra<sup>1, a)</sup>

*Department of Chemistry,  
Indian Institute of Technology Bombay,  
Powai, Mumbai 400076, India*

(Dated: 8 February 2023)

Recent advancements in quantum information and quantum technology has stimulated a good deal of interest in the development of quantum algorithms for energetics and properties of many-fermionic systems. While the variational quantum eigensolver is the most optimal algorithm in the Noisy Intermediate Scale Quantum era, it is imperative to develop low depth quantum circuits that are physically realizable in quantum devices. Within the unitary coupled cluster framework, we develop COMPASS, a disentangled ansatz construction protocol that can dynamically tailor an optimal ansatz using the one and two-body cluster operators and a selection of rank-two scatterers. The construction of the ansatz may potentially be performed in parallel quantum architecture through energy sorting and operator commutativity prescreening. With significant reduction in the circuit depth towards the simulation of molecular strong correlation, COMPASS is shown to be highly accurate and resilient to the noisy circumstances of the near-term quantum hardware.

## I. INTRODUCTION

The determination of atomic and molecular energetics and properties is one of the most anticipated applications of quantum computing in near term quantum computers. With the advent of coherent multiple qubit quantum processors, the problem with the exponential growth of the Hilbert space that one often encounters in many-body physics and chemistry can be handled in a tractable manner. While the limited coherence time and poor gate fidelity are major impediments towards the implementation of quantum many-body methods in Noisy Intermediate Scale Quantum (NISQ) devices, nonetheless, one cannot deny the importance of designing methods and algorithms that are realizable on quantum computers to span many-body Hilbert space<sup>1-3</sup>.

Historically, the quantum phase estimation algorithm (QPEA), proposed by Abrams and Lloyd<sup>4,5</sup>, was the first quantum algorithm towards the simulation of state energies of a many-fermionic system. QPEA relies on the construction of an input reference state that is projected onto the target eigenstate via a unitary operation<sup>6-8</sup>. Although theoretically appealing, the long coherence time required for the such unitary evolution due to extremely deep and complex quantum circuits warrants the availability of sufficiently large number of fault-tolerant qubits which is still beyond experimental realization. The variational quantum eigensolver<sup>9</sup> provides a lucrative alternative platform for the digital simulation of quantum many-body systems in NISQ devices.

VQE has been realized experimentally in various quantum hardware architectures like the photonic quantum processors<sup>9</sup>, superconducting quantum processors<sup>10</sup> and trapped ion architectures<sup>11</sup>. Significant theoretical developments of VQE tailored for various hardware platforms immediately followed its experimental demonstration. VQE presumes the prior knowledge of the many-body Hamiltonian matrix ele-

ments from the classically computed values and aims to finding the "best" variational approximation to the ground state wavefunction of the Hamiltonian starting from a trial wavefunction Ansatz. The trial wavefunction is constructed in terms of a series of tunable parameters which provide its variational flexibility. The state of the system is prepared through a parametrized quantum circuit, followed by computing the expectation value of the Hamiltonian through repeated measurements. Both these steps are carried out in quantum hardware while the update of the parameters take place via some classical optimization in classical hardware. The attractive feature of VQE is that the state preparation can be done via shorter quantum circuits compared to QPEA, making it a more desirable candidate for NISQ devices. Needless to say, the VQE results and the associated energy landscape often depend critically on the choice of the parametrized ansatz<sup>3,12,13</sup>.

One of the most significant developments towards the practical realization of the unitary evolution in a quantum computer directly originated from the unitary variant of coupled cluster theory (UCC)<sup>9,14-18</sup> with a given truncation in the rank of the cluster expansion. While the UCC ansatz with single and double excitation operators (UCCSD) provides a compact wavefunction ansatz, they work best in the cases where the molecular non-dynamic correlation is somewhat weak. Several efforts have been made to make the UCC work for areas of strong correlation, either by increasing the excitation rank at the expense of higher implementation overhead or by including generalized hamiltonian matrix elements in the wavefunction parametrization. The latter class of methods stems from Nakatsuji's density theorem<sup>19</sup> and Nooijen's conjecture<sup>20</sup> about the possibility of expressing the eigenstates of a Hamiltonian containing one and two body terms in terms of generalized excitation operators. While theoretically exact, a direct VQE implementation with all generalized<sup>21</sup> excitation operators incurs high implementation cost which is far beyond NISQ realization. The excitation list can further be pruned by keeping only generalized paired terms, giving rise to k-UpCCGSD ansatz<sup>21</sup> for which the circuit depth grows only linearly with the system size. In a different approach, the

<sup>a)</sup>Electronic mail: rmaitra@chem.iitb.ac.in

present authors proposed a partially disentangled form of the unitary in which the high rank excitations are implicitly folded in through nested commutators of two-body scattering operators with effective hole-particle excitation rank of one and the standard cluster operators<sup>22</sup>.

The goal for an expressive ansatz is to span the  $N$ -electron Hilbert space through a set of connected operators, ideally of rank  $N$  at max. While keeping the maximum rank of the operators (that enter the parametrization) two for better NISQ realization, one must be able to express any  $N$ -body connected hole-particle excitation through low power cumulative actions of different non-commuting operators<sup>23,24</sup>. The action of any generalized operator with effective excitation rank zero on functions of the so-called *primary excitation subspace* (spanned by the set of  $n$ -tuply excited determinants; *vide infra*) either leads to nilpotent solution, or results in redundant functions within the primary excitation subspace. The two-body operator with effective excitation rank one (to be referred as scattering operator or scatterers, henceforth) can of course recursively lead to  $(n+1), (n+2), (n+3) \dots$ -tuply excited functions to span the secondary excitation subspace. However, for such non-trivial action to exist, the specific scatterer (that leads to a determinant of the secondary excitation subspace by its action on a given primary excited determinant) must not commute with the cluster operator which generates the primary excitation function. As such, in this work, we pre-screen the scatterers on-the-fly in terms of their (non-)commutativity with the cluster operators to come up with a dynamically optimal solution protocol: the COMmutativity Pre-screened Automated Selection of Scatterers (COMPASS). COMPASS can be implemented in a parallel quantum architecture to choose the energetically most significant cluster operators to span the primary excitation manifold and select the scatterers from an operator bath based on the commutativity criteria to span the secondary excitation manifold. The entire ansatz may be constructed in a parallel quantum environment and can be implemented with extremely shallow quantum circuit.

Following the discussions on the genesis of COMPASS, we would discuss its performance for the cases of molecular strong correlation in which conventional UCCSD fails to achieve desirable accuracy. In particular, we would study the accuracy of COMPASS in handling molecular strong correlation, vis-a-vis the number of parameters needed. Furthermore, we would analyse the accuracy of COMPASS in the case of noisy simulations to demonstrate its expected performance in faulty quantum devices and would argue its suitability as a leading candidate for NISQ realization.

## II. THEORY

### A. Choice of the Operators Class and Motivation towards the Genesis of COMPASS:

In order to design a compact parametrized ansatz, the choice of the operators play the pivotal role. As discussed in the introduction, we choose to work with a set of one and two-

body cluster operators along with a set of scatterers. The scatterers are two-body operators with effective hole-particle excitation rank one and have one quasi-hole or quasi-particle "destruction operator". Each element of the scatterers is equipped with an in-built projector such that it has non-trivial action on only a selected set of primary excitation subspace determinants:

$$S_h = \frac{1}{2} \sum_{ami j} s_{ij}^{am} \{a^\dagger m^\dagger ji\} |\dots i \dots j \dots m \dots \rangle \langle \dots \bar{a} \dots \bar{m} \dots j \dots i \dots | \quad (1)$$

$$S_p = \frac{1}{2} \sum_{abie} s_{ie}^{ab} \{a^\dagger b^\dagger ei\} |\dots i \dots e \dots \bar{a} \dots \bar{b} \dots \rangle \langle \dots \bar{b} \dots \bar{a} \dots e \dots i \dots | \quad (2)$$

Here,  $a, b, c, \dots$ , etc. denote the set of unoccupied particle orbitals and  $i, j, k, \dots$ , etc. are the set of occupied hole orbitals with respect to the HF vacuum. Note that, ' $m$ ' is a hole state and ' $e$ ' is a particle state with respect to HF vacuum and they together form a contractible set of orbitals (CSO). The orbitals constituting CSO appear as the quasi-hole and quasi-particle destruction operators in  $S$ . Thus, the operator  $S$  that contains the label  $m$  (or  $e$ ) may be denoted as  $S^m$  (or  $S_e$ ). Similarly, the cluster operator  $T$  with orbital label  $m$  (or  $e$ ) may be denoted as  $T_m$  (or  $S^e$ ). Note that for the cluster operators, both  $m$  ( $e$ ) appears as quasi-hole (quasi-particle) *creation* operators whereas they appear as *destruction* operators in  $S$ . As such, the contractions between  $S$  and  $T$  take place through them to simulate a higher excitation rank operator. Each contraction between the scatterers and the cluster operators increases the effective hole-particle ex-

citation rank by one, for example,  $\overline{ST_2} \rightarrow T_3$ ,  $\overline{SST_2} \rightarrow T_4 \dots$ . The anti hermitian counterpart of the  $S$  and  $T$  operators ( $\sigma = S - S^\dagger$ ;  $\tau = T - T^\dagger$ ) may be used to construct a unitary evolution operator which can be implemented in quantum architecture. With the knowledge of the (non-)commutativity among various  $\sigma^m = S^m - S^{m\dagger}$  and  $\tau_m = T_m - T_m^\dagger$  (and among  $\sigma_e = S_e - S_e^\dagger$  and  $\tau^e = T^e - T^{e\dagger}$ ), the effects of connected high rank excitations can be built through nested commutators like  $[\sigma, \tau_2] \rightarrow \tau_3$ ;  $[[\sigma, \tau_2], \tau_2] \rightarrow \tau_4 \dots$  and so on. As such a partially disentangled (factorized) ansatz can be shown to include the infinite commutators even when a finite Trotter order<sup>25</sup> is used to approximate  $e^\tau$  and/or  $e^\sigma$ .

$$e^\sigma \cdot e^\tau = e^{\sigma + \tau + [\sigma, \tau] + [[\sigma, \tau], \tau] + \dots} \quad (3)$$

Note that the action of the unitary  $e^\sigma$  on the  $e^\tau |\Phi_{HF}\rangle$  is partially nilpotent due to the inbuilt projector in the definition of  $\sigma$ . Expanding the entangled states  $e^\tau |\Phi_{HF}\rangle$  in terms of constituent zero, one, two, ... body excited determinants (which belong to the primary excitation manifold), one may write

$$e^\sigma (e^\tau |\Phi_{HF}\rangle) \rightarrow e^\sigma (|\Phi_{HF}\rangle + \sum c_I |\Phi_I\rangle) \quad (4)$$

Here  $\Phi_I$ 's are the various determinants belonging to the primary excitation manifold generated by  $e^\tau |\Phi_{HF}\rangle$ . The index  $I$  would generically denote the composite hole-particle indices

associated with the excited determinants or with the cluster operators. Note that each  $\sigma$  operator is characterized by a quasi-hole/particle destruction operator that belongs to CSO. The action of  $\sigma$  is nontrivial only on certain set of primary subspace determinants. For example, a  $\sigma$  operator with quasi-hole destruction orbital ' $m$ ' acts only on those excited primary subspace determinants where the occupancy of ' $m$ ',  $n_m$  is zero. For each  $\sigma^m$ , the occupancy of ' $m$ ' may be used to divide the primary subspace determinants on which  $\sigma^m$  acts into two sets.

$$\sum_I c_I |\Phi_I\rangle = \sum_{J=1}^{N_1} c_J |\Phi_J(n_m=0)\rangle + \sum_{K=1}^{N_2} c_K |\Phi_K(n_m=1)\rangle \quad (5)$$

with  $N = N_1 + N_2$  represents the total number of determinants generated by  $e^\tau |\Phi_{HF}\rangle$  that span the primary subspace. Note that for a hole state ' $m$ ',  $e^{\sigma^m}(\sum_J c_J |\Phi_J(n_m=0)\rangle)$  has non-vanishing action while  $e^{\sigma^m}(\sum_K c_K |\Phi_K(n_m=1)\rangle)$  is nilpotent. These determinants with  $n_m = 0$  are principally generated by  $\tau_m$  and these cluster operators do not commute with  $\sigma^m$ . Unfortunately, an unrestricted construction of the entangled state  $\sum_I c_I |\Phi_I(n_m=0 \oplus n_m=1)\rangle$  utilizes high number of parameters, resulting in a deep circuit. An exact similar analysis can be done when the destruction operator is a quasi-particle state that belongs to CSO.

Instead, one may selectively generate only those primary subspace determinants by the cluster operators on which the scatterers have a non-trivial action. The COMPASS dynamically chooses the "best" set of cluster amplitudes in a factorized manner. Each of the primary subspace determinants, generated by the individual cluster amplitudes, are scanned for whether a non-commuting scatterer (with which the corresponding cluster operator share CSO) have significant effect or not. Where the commutativity criteria is met, the scatterers are immediately allowed to act upon the entangled state. In the next section, we would present the genesis of COMPASS and discuss upon how it directs to the construction of the most optimal ansatz.

## B. Development of COMPASS: an Automated Toolkit for Dynamic Ansatz Design

COMPASS relies on the choice of the "best" set of the cluster operators and selection of the appropriate scatterers that have significant contribution by their action on certain entangled states. The whole ansatz is constructed dynamically, possibly in a parallel quantum architecture and the resulting ansatz features as a disentangled product of various  $e^{\sigma^\mu}$  and  $e^{\tau^\nu}$  in an interwoven manner. As mentioned before, the indices  $I, J, K, L, \dots$  are used to denote the composite excitation labels associated with  $\tau$  whereas  $\mu, \nu, \lambda$  would denote the composite orbital labels for  $\sigma$ . COMPASS consists of three components: a parallel selection of the "best" amplitudes and energy ordering, selection of the appropriate scatterers from an operator bath via CSO scanning, and the preparation of the final ansatz. A schematic figure of COMPASS is presented in Fig 1 and the details of the same is discussed below.

### 1. Choice of the "best" cluster operators and the ordering of their appearance:

The choice of the "most important" cluster operators is a key step to design a shallow depth quantum circuit in the NISQ devices<sup>26</sup>. Towards this, we have considered only the double excitation operators (generically to be denoted as  $\tau_d$ ) while the single excitation cluster operators (generically to be denoted as  $\tau_s$ ) will be handled separately. With the availability of multiple quantum devices, one may parallelly optimize the various one parameter energy functional:

$$\begin{aligned} E_I &= \langle \Psi(\theta_I) | \hat{H} | \Psi(\theta_I) \rangle, \\ &= \langle \Psi_{HF} | e^{-\tau_I} H e^{\tau_I} | \Psi_{HF} \rangle \\ &\quad \forall I \in (1, n_o^2 n_v^2) \end{aligned} \quad (6)$$

Each of these can be done through a one parameter circuit, with  $\theta_I$  being the sole variational parameter. Here  $|\Psi(\theta_I)\rangle = e^{\tau_I(\theta_I)} |\Psi_{HF}\rangle$ . If sufficiently large number of quantum computers are available, each  $E_I$  can be evaluated on different devices simultaneously. Otherwise, on a single quantum device one may repeat this multiple times and take an average of  $E_I$ . Only those  $\tau_I$  operators will be kept in the cluster operator pool for which  $\Delta E_I = |E_I - E_{HF}| > \epsilon_1$ , where  $\epsilon_1$  is a predefined threshold and the rest of the cluster operators are discarded.

With the  $N_T$  number of cluster operators that pass through the energy screening, we align them in a descending order of their contribution to correlation energy. Energetically most contributing cluster operator is allowed to act on the HF state directly, followed by the next and so on. This implies that for  $N_T$  cluster operators with  $\dots \Delta E_J > \dots > \Delta E_K > \dots > \Delta E_L \dots$ ,  $e^{\tau_J}$  is placed in operator block  $\beta$ ,  $e^{\tau_K}$  in operator block  $\gamma$ , ... and so on in a disentangled manner. Note that  $\dots \delta > \dots > \gamma > \dots > \beta > \dots > 1$

$$\begin{aligned} |\Psi\rangle &= \dots [e^{\tau_L}]_\delta \dots [e^{\tau_K}]_\gamma \dots [e^{\tau_J}]_\beta \dots |\Psi_{HF}\rangle \\ |\Psi\rangle &= \prod_{\alpha=1}^{N_T} [e^{\tau_I}]_\alpha |\Psi_{HF}\rangle \end{aligned} \quad (7)$$

where the quantities inside parenthesis denote the order of the operator blocks in which they act on  $|\Psi_{HF}\rangle$ . This ordering will be maintained throughout. In general, if a given  $\tau_I$  is placed in operator block  $[\dots]_\alpha$ , we would denote it as  $[\tau_I]_\alpha$ . We mention that each cluster operator is allowed to appear only once irrespective of the block it is placed. In the next subsection, we will dynamically expand the operator blocks by placing the scatterers appropriately based on the commonality of CSO labels shared between the cluster operators and the scatterers.

### 2. Selection of the Scatterers from Operator Bath

For each operator  $[\tau_I]_\alpha$  selected through the energy screening, one first checks if  $\tau_I$  contains any orbital that belongs to CSO. For the cluster operators which do not contain any index of CSO, the corresponding operator block is not expanded

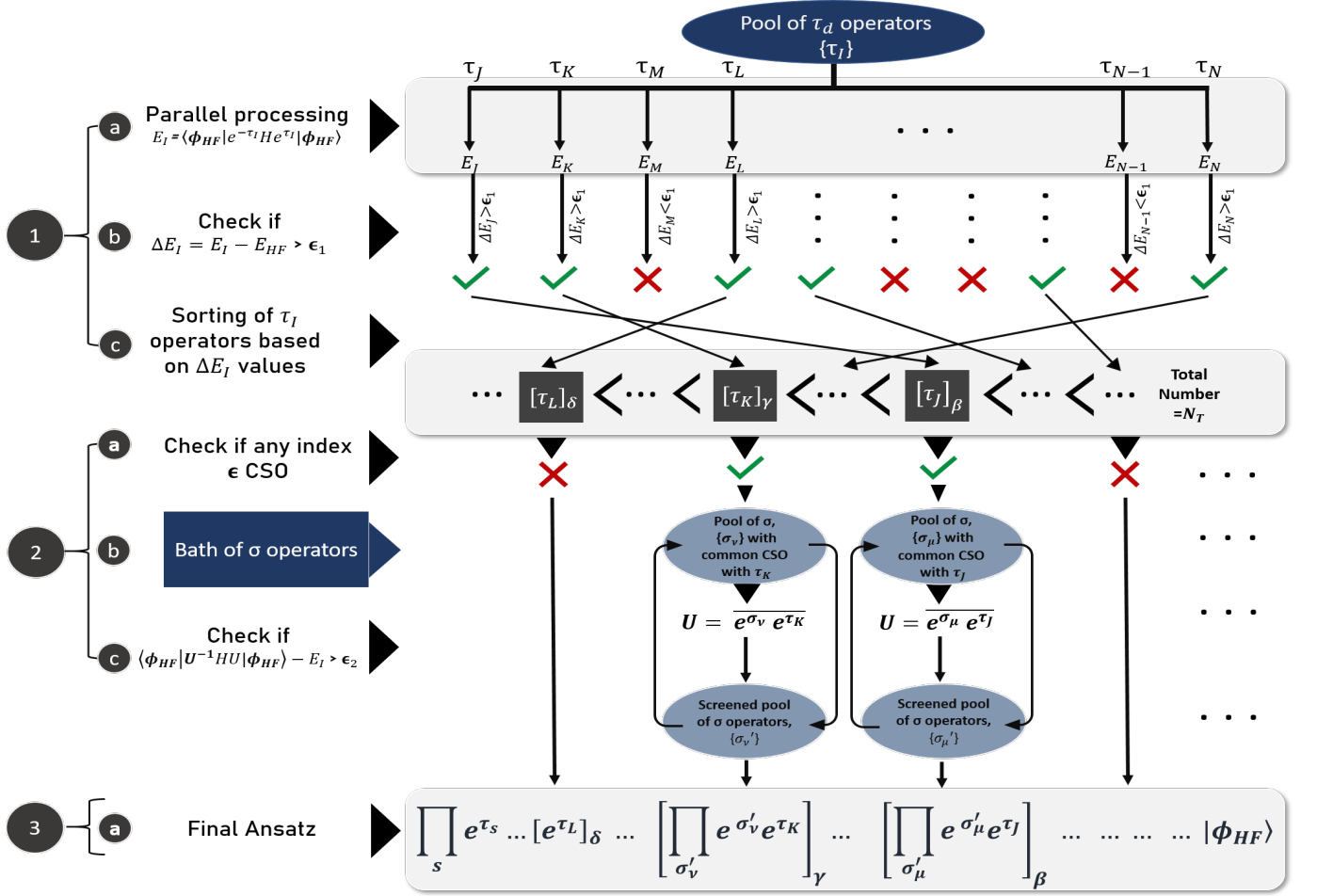


FIG. 1: Schematic representation of COMPASS protocol. In step 1(a-c), each cluster operator  $\tau$  is screened (potentially in a massively parallel quantum architecture) through a threshold criteria and kept in an operator block as per their descending contribution to correlation energy. Each such selected  $\tau$  is checked if that contains any orbital(s) that belongs to CSO (step 2(a)). For each operator block with selected  $\tau$  operator, appropriate non-commuting  $\sigma$  operator(s) are fetched from the operator bath. The blocks are expanded by including the energetically dominant  $\sigma$  operators (denoted in this figure as  $\sigma'$ ), one at a time, selected via the optimization of two-parameter energy functionals (step 2(b)). This step can again be performed in a parallel quantum architecture. The operator bath, in principle, may supply infinite number of  $\sigma$  operators and is never drained out. The final ansatz is constructed by concatenating the various operator blocks, keeping the ordering unchanged (step 3(a)).

any further. For all other cluster operators with one or more orbitals that belongs to CSO, a pool of scatterers is created from the scatterer bath through commutativity screening. This implies that the cluster operator and the scatterers should contain the same set of contractible orbital(s). Thus for a given  $[\tau_{m_l}]_\alpha$ , the scatterer pool contains all the operators of the structure like  $\sigma^m$ . With  $N_\alpha$  number of such scatterer selected in the pool (corresponding to the operator block  $\alpha$  containing  $\tau_l$ ), one optimizes the following two parameter energy functional:

$$\begin{aligned} E_{l\mu} &= \langle \Psi(\theta_l, \theta_\mu) | \hat{H} | \Psi(\theta_l, \theta_\mu) \rangle, \\ &= \langle \Psi_{HF} | e^{-\tau_l} e^{-\sigma_\mu} H e^{\sigma_\mu} e^{\tau_l} | \Psi_{HF} \rangle \\ &\quad \forall \mu \in (1, N_\alpha) \end{aligned} \quad (8)$$

Here the overline suggests the connected action of  $\tau_l$  and the various  $\sigma_\mu$ 's that share *at least* one common orbital index that

belongs to CSO. However, only those scatterers are screened for which  $|E_{l\mu} - E_l| > \epsilon_2$ , where  $\epsilon_2$  is a predefined threshold whose value is usually taken to be order of magnitude less than  $\epsilon_1$ . With the energy condition met, the operator block  $[\dots]_\alpha$  is expanded by including appropriate  $\sigma_\mu$ 's through disentangled (factorized) unitary.

$$U_\alpha = \left[ \prod_\mu e^{\sigma_\mu} e^{\tau_l} \right]_\alpha \quad (9)$$

There may, of course, be specific cases where the  $\tau$  operator in a given operator block does not contain any orbital of CSO and in that case, as mentioned before, no  $\sigma$  gets attached to it. However, it still gets placed according to its energy ordering. Note that, for general cases, with each  $\sigma_\mu$  being selected one-by-one for a given  $\tau_l$ , the optimization in Eq. 8 can be done

with shallow two-parameter circuit with  $\theta_I, \theta_\mu$  as the two variational parameters. One may further note that the selection of scatterers for various operator blocks are independent of each other and thus the evaluation of  $E_{I\mu}$  in Eq. 8 for various pairs of  $\tau_I$  and  $\sigma_\mu$  can be done with multi-level parallelization. Furthermore, if sufficiently large number of quantum computers are available, one may evaluate the energy functional  $E_{I\mu}$  in different devices simultaneously or otherwise, one may perform it multiple times in a single quantum device and take an average value. We further note that while a given  $\tau_I$  appears only once in the ansatz, a given  $\sigma_\mu$  may be attached to various  $\tau_I$ 's in their respective operator blocks and thus the  $\sigma$  operators are never drained out from the operator bath.

### 3. Weaving the Final Ansatz

The final ansatz is constructed by concatenating the various operator blocks. As mentioned above, depending on the commonality of the contractible orbitals between the  $\tau$  and  $\sigma$  operators, several  $\tau_I$  operator may attach same  $\sigma$  operator to appear in their respective operator blocks. Finally, all the one-body cluster operators,  $\tau_s$ , are placed at the end in lexical ordering.

$$U = \prod_s e^{\tau_s} \prod_\alpha U_\alpha \quad (10)$$

Once the full ansatz is constructed for a given molecule with a fixed nuclear arrangement, the parameters involved in the ansatz, Eq. 10 are optimized using the standard VQE hybrid quantum-classical framework till all the parameters are converged.

One may note that the proposed ansatz may span the entire  $N$ -electron Hilbert space. However, in COMPASS each  $\sigma$  operator is chosen and clubbed with one or more non-commuting  $\tau$  operator(s) in a way that lowers the correlation energy beyond a certain predefined threshold. The selected  $\sigma$  operators are allowed to act immediately upon certain entangled states that are generated by the action of the associated non-commuting  $\tau$  on the Hartree Fock determinant. Note that only those  $\sigma$  operators are kept in a given operator block (having a pre-selected cluster operator  $\tau$ ) that can generate at least a triply excited secondary excitation subspace function.

## III. RESULTS:

COMPASS has been implemented with an interface to qiskit-nature<sup>27</sup> which imports the one and two-electron integrals from PySCF<sup>28</sup>. All the calculations performed in this study employed STO-3G basis set<sup>29</sup> with a direct spinorbital to qubit mapping. The Jordan-Wigner transformation<sup>30</sup> was employed to encode second quantized operators to qubit operators. For all our calculations, we chose the L-BFGS-B<sup>31,32</sup> optimizer for the classical optimization. Also, we had initialized the qubits to the Hartree-Fock reference state and each parameters of the ansatz was initialized to the optimized val-

ues obtained from the minimization of energy functional of Eq.8 (and Eq. 6).

While the  $\sigma$  operators generically used so far towards the development have all possible spin- and spatially-unrestricted terms in it, in the actual implementation, the list is further significantly pruned by keeping only a few specific kinds of the same. Two different cases are considered which are different from each other in the choice of the  $\sigma$  operator taken in the operator bath. In particular, we have worked with the (a) opposite spin (OP) sector of  $\sigma$  and (b) the partially paired (PP) sector of  $\sigma$ .

The OP sector incorporates the specific low-spin channel of  $\sigma$ . This implies that the spins in the excitation vertex and the scattering vertex of are different.

$$\sigma_{OP} \in \{(\sigma_h)_{i_\alpha j_\beta}^{a_\alpha u_\beta}, (\sigma_h)_{i_\beta j_\alpha}^{a_\beta u_\alpha}; (\sigma_p)_{i_\alpha v_\beta}^{a_\alpha b_\beta}, (\sigma_p)_{i_\beta v_\alpha}^{a_\beta b_\alpha}\} \quad (11)$$

$u$  and  $v$  are the spatial active hole and virtual orbitals that form the CSO, and  $\alpha$  and  $\beta$  denote the spin-up and spin-down electrons, respectively.

The PP sector of  $\sigma$  includes (i) only those quasi-hole creation operators which originate from the same spatial orbitals (for  $\sigma_h$ ) and (ii) only those quasi-particle creation operators which share the same spatial orbitals (for  $\sigma_p$ ).

$$\sigma_{PP} \in \{(\sigma_h)_{i_\alpha i_\beta}^{a_\alpha u_\beta}, (\sigma_h)_{i_\beta i_\alpha}^{a_\beta u_\alpha}; (\sigma_p)_{i_\alpha v_\beta}^{a_\alpha a_\beta}, (\sigma_p)_{i_\beta v_\alpha}^{a_\beta a_\alpha}\} \quad (12)$$

Irrespective of the choice of the sector of  $\sigma$ , the orbitals constituting CSO are restricted only to those that span the chemically active region.

As discussed previously, COMPASS uses two threshold parameters ( $\epsilon_1$  and  $\epsilon_2$ ) which ensure to include the most dominant cluster amplitudes and the scatterers in the final ansatz. As such, COMPASS calculations with thresholds of  $\epsilon_1$  and  $\epsilon_2$  would be denoted as COMPASS( $-\log(\epsilon_1), -\log(\epsilon_2)$ ).

### A. Accuracy vs Parameter Count over the Potential Energy Profile of Strongly Correlated Molecules:

Towards the study of the accuracy of COMPASS, three difficult test cases have been identified: the potential energy surface for the stretching of  $BH$  single bond, the symmetric simultaneous single bond stretching of  $H_2O$  and linear  $BeH_2$ . In all cases, the results are compared against UCCSD. In all our calculations, all the amplitudes corresponding to the spin-complemented operators are treated as independent.

Stretching of the single bond in  $BH$  is one of the most difficult test cases for assessing the accuracy of any quantum many-body theory. The system shows the signature of strong molecular correlation due to the interplay of the ground and excited roots when the  $B-H$  bond is stretched. We model its dissociation profile with COMPASS and UCCSD.  $BH$  consists of 6 electrons in 12 spinorbitals with a total Hilbert space dimension of 4096. The UCCSD energy profile, when plotted as a function of  $B-H$  distance shows energy error  $\sim 1$  kcal/mol with respect to the classically exact Full Configuration Interaction (FCI) method throughout various molecular arrangements. COMPASS with both the variants, OP and PP,

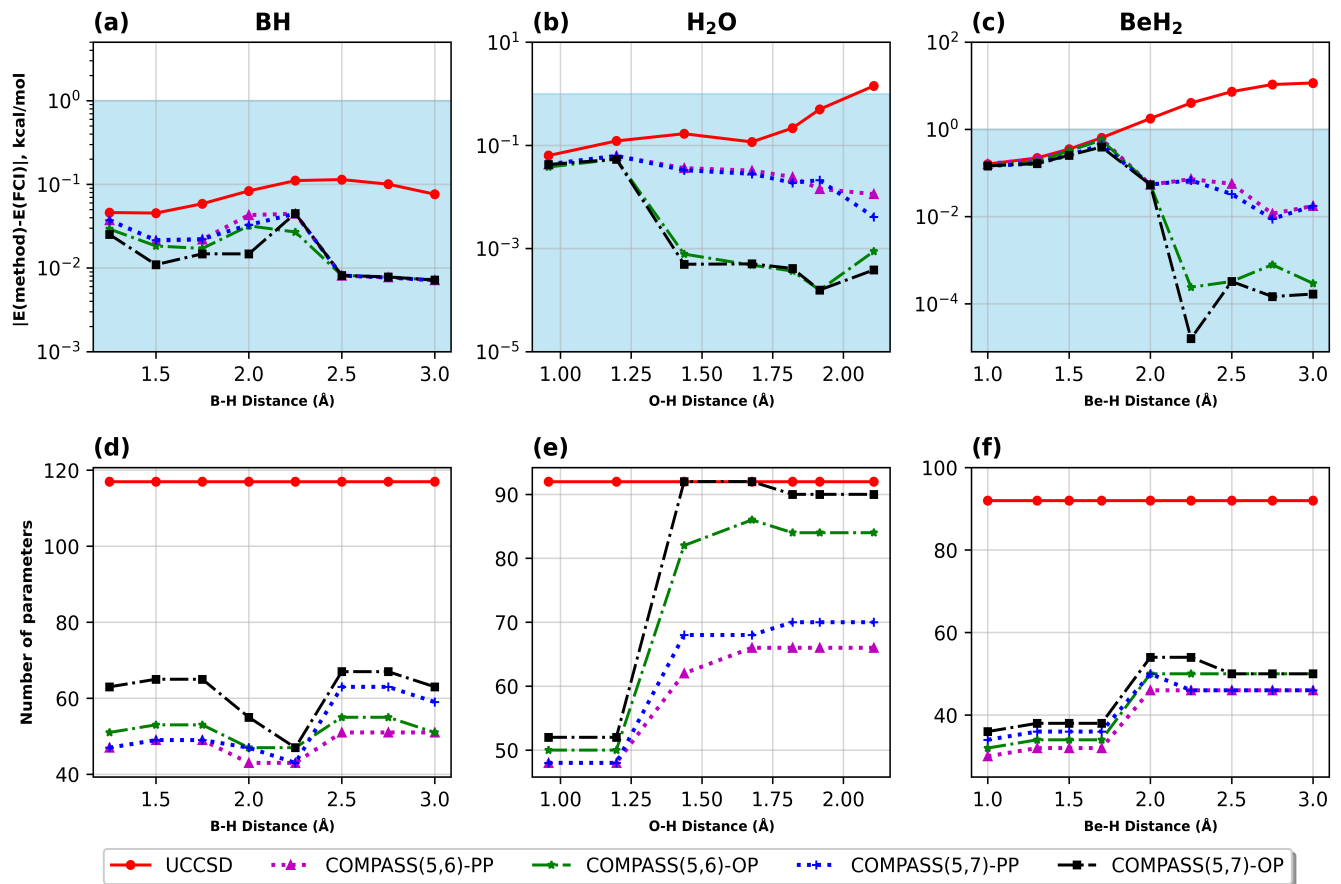


FIG. 2: Accuracy as a function of the bond length parameter for various versions of COMPASS with respect to FCI: (a)  $BH$ , (b)  $H_2O$ , and (c) linear  $BeH_2$ . The region shaded in pale blue indicates chemical accuracy in kcal/mol. (d), (e) and (f) estimate parameter counts for  $BH$ ,  $H_2O$  and linear  $BeH_2$ , respectively, along the potential energy profile.

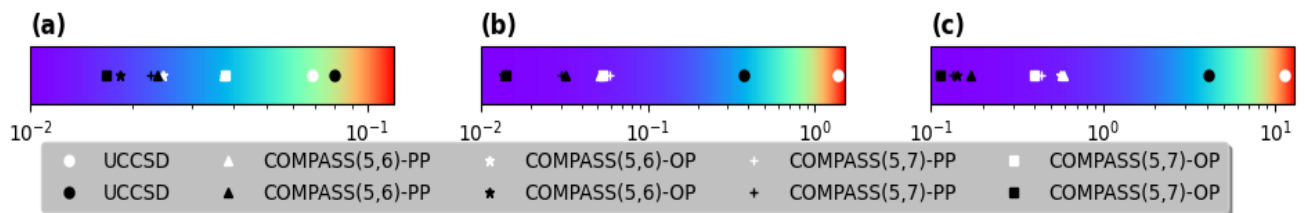


FIG. 3: NPE (white symbols) and average error (black symbols) (in kcal/mol) across the potential energy profile for (a)  $BH$ , (b)  $H_2O$ , and (c) linear  $BeH_2$  models. For  $H_2O$ , the NPE shows two orders of magnitude improvement over the UCCSD while for the linear  $BeH_2$ , all variants of COMPASS have several orders of magnitude improvement in NPE, estimating a uniform description of many-body correlation effects over the entire energy profile. The color-coded horizontal axis denotes the order of NPE and average errors.

outperform UCCSD throughout the energy surface and particularly when the molecule is sufficiently stretched, it shows improvement by an order of magnitude. Interestingly enough, COMPASS(5,7) with OP variant takes about 67 parameters at bond length of 2.5 and 2.75 Å, which is the highest (compared to other nuclear arrangements) in terms of the number of parameters required for COMPASS, but still this is an order of magnitude less than the 117 parameters (without combin-

ing the spin-complementary excitations) taken up by UCCSD. The accuracy throughout the potential energy profile is also illustratively evident from the non-parallelity error (NPE) and the average error for various schemes and is shown in Fig. 3(a).

$H_2O$  in STO-3G basis, with one core spatial orbital frozen, renders to be a system with 8 electrons in 12 spinorbitals. In Fig. 2b, we have plotted the energy error with respect

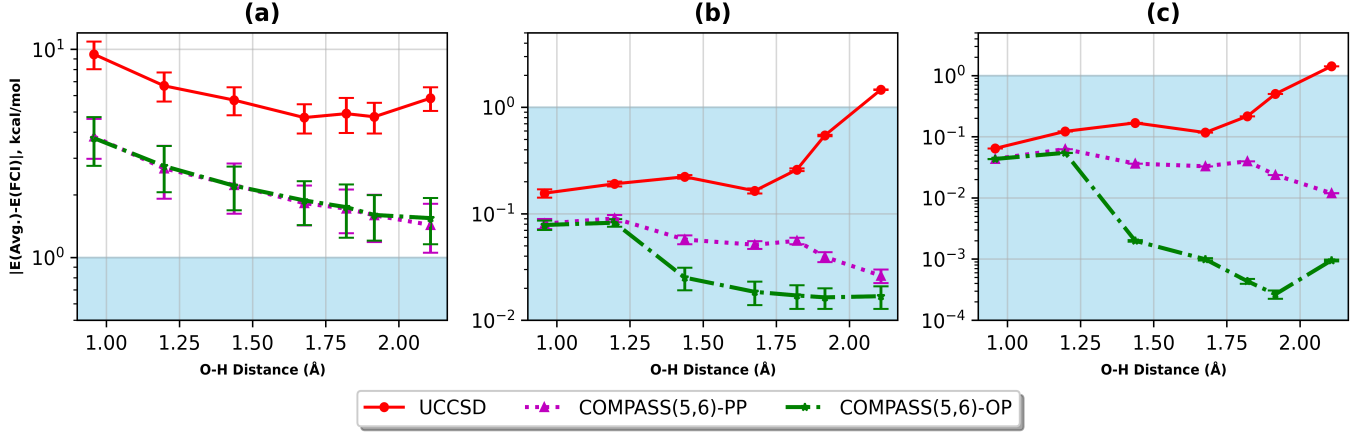


FIG. 4: Accuracy as a function of bond length parameters for  $H_2O$  ( $H - O - H = 104.4776^\circ$ ) under gaussian noise model characterized by standard deviation  $SD$ : (a)  $SD = 10^{-2}$ , (b)  $SD = 10^{-3}$ , (c)  $SD = 10^{-4}$ . For both (b) and (c) the average energy predicted by COMPASS are well within chemical accuracy. For all the variants, COMPASS predicts energy which are at least an order of magnitude accurate than UCCSD across the energy profile; demonstrating its resilience to noisy environment. The vertical lines across each point suggest the standard deviation of the observed energy values with 100 independent samples.

to FCI method as a function of the bond length parameter keeping the  $H - O - H$  angle fixed at  $104.4776^\circ$ . While the UCCSD ansatz requires 92 parameters (without combining the spin- complementary excitations), it fails to achieve energy error within chemical accuracy when the bonds are sufficiently stretched. Dramatically enough, all the variants of COMPASS with different threshold parameters significantly outperforms UCCSD and resulting COMPASS energy values are just a few micro-Hartree away from FCI throughout the energy surface. Even more impressive is the significantly fewer number of parameters selected by most of the COMPASS variants to achieve this level of accuracy throughout the potential energy profile: COMPASS(5,6) with the PP variant barely needs about 66 parameters, resulting in a much compact form of the wavefunction ansatz. Beyond  $1.4 \text{ \AA}$ , OP variants require higher number of parameters than the PP counterpart; however, this also results in at least an order of magnitude improvement in accuracy. The overall superiority of COMPASS in comparison to UCCSD is again measured in terms of NPE and the average error and is demonstrated in Fig. 3(b).

The efficacy of COMPASS is much more pronounced in strongly correlated systems like a linear  $H - Be - H$  model when we simultaneously stretch the  $Be - H$  bonds in a symmetric manner. Due to the strong electronic correlation on symmetric stretching of the bonds, the UCCSD behaves somewhat poorly and beyond  $R_{Be-H} = 1.75 \text{ \AA}$ , its energy error with respect to FCI goes beyond 1 kcal/mol. The error further increases on further stretching the bonds, marking a clear signature of strong correlation. COMPASS with all the variants show remarkable improvement over UCCSD results with at least one order of magnitude in the region of short  $R_{Be-H}$  length and by several orders of magnitude when the bonds are further stretched. This comes at a remarkable reduction

in the number of parameter count over UCCSD: in the worst case scenario, COMPASS(5,7) with OP variant utilises about 54 parameters around  $R_{Be-H} = 2.00 - 2.25 \text{ \AA}$ , while UCCSD requires 92 parameters. In fact, the OP variant shows several order of magnitude improvement in accuracy over the PP variant, particularly in regions beyond  $2 \text{ \AA}$ . However, for two different sets of  $\epsilon_1$  and  $\epsilon_2$ , both COMPASS-OP and COMPASS-PP require similar number of parameters throughout the potential energy profile. The extremely high accuracy over the potential energy profile is again measured in terms of the NPE and average error (Fig. 3(c)) and COMPASS variants show clear two orders of magnitude improvement of these metrics over UCCSD. The accuracy and parameter count in linear  $BeH_2$  model clearly demonstrate the performance of COMPASS in compactifying the ansatz for the simulation of strong electronic correlation, making it more suitable for NISQ realization.

## B. Simulation with Gaussian Noise Model:

The simulation so far has presumed a noiseless implementation in an ideal quantum environment. However, the NISQ devices are not fault-tolerant and as such in practical scenario, one needs to account for the uncertainties due to imperfect implementation. Towards this, for each set of optimal parameters generated in an ideal quantum setting, we randomly produce 100 samples of noisy parameters derived via a Gaussian distribution model<sup>33,34</sup>. For each parameter, the distribution is centered at the optimal parameter value and the noisy parameters ( $\theta_m$ ) are generated as:

$$\theta_m = \exp\left(-\frac{(\theta - \theta_n)^2}{2(SD)^2}\right) \quad (13)$$



Here  $\theta_n$  is the optimal value of the parameters and  $SD$  is the standard deviation. Three different cases are considered with  $SD = 10^{-2}$ ,  $SD = 10^{-3}$  and  $SD = 10^{-4}$ . With each of the 100 samples taken into account for various  $SD$ , we estimate the average energy.

To estimate the performance of COMPASS with imprecise implementation of the parameters, we choose to work with  $H_2O$  with the same set of geometrical parameters as in the case discussed earlier. We took a conservative COMPASS parameters  $\epsilon_1 = 10^{-5}$ ,  $\epsilon_2 = 10^{-6}$ . In all various noise strengths, the different variants of COMPASS seem to be more resilient than UCCSD. With low noise strength ( $SD = 10^{-4}$ ,  $SD = 10^{-3}$ ), in the regions where the bonds are sufficiently stretched and the strong correlation dominates, COMPASS variants are clearly a few orders of magnitude more accurate than the UCCSD counterpart (Fig. 4b, c). Only in the case of reasonably strong noise with  $SD = 10^{-2}$ , COMPASS fails to achieve chemical accuracy though it is about an order of magnitude more accurate than UCCSD. One may note that in cases of such noisy simulations, the optimal parameters are of the same order of magnitude as the noise itself, and this may not potentially cause a hindrance to its realistic implementation.

#### IV. DISCUSSION AND FUTURE OUTLOOK:

Being a dynamic structured ansatz, it is difficult to comment on the resource requirements and the computational cost of COMPASS. The measure for the resource requirement for a NISQ device is often taken to be the circuit depth and the number of measurements. While the number of measurement is an important parameter that determines the overall time to the solution, for a NISQ realization, the circuit depth may be taken as the most important metric. One may note that the latter determines the feasibility of implementation of the algorithm in devices with short coherence time.

The parent VQE algorithm suffers from the limitation of large number of measurements required to reach the solution. The COMPASS algorithm is likely to suffer from the same drawback, if not slightly more. This mainly is due to the (a) the ansatz construction (step 1,2, Fig. 1) and (b) optimization of the final ansatz. One may note that the ansatz construction only requires several one and two-parameter energy functional optimization. Each of such optimization require very few number of iterations and hence they involve few measurements. Most importantly, each of these energy optimizations are independent and thus can be performed in parallel quantum architecture. Thus, with the development of hardware capabilities, the requirement of increased number of shot count during the ansatz construction is likely to pose limited challenges. However, the amplitude optimization towards the final state preparation may take somewhat more number of steps (than standard UCCSD) due to the generalized operators present in the ansatz, resulting in a slower convergence. This is principally attributed to the classical optimizer and one may adopt various strategies to accelerate. The development of the fastest convergence algorithm would be studied in near future as it requires several aspects to take care of.

We must point out that COMPASS is conceptually entirely different than the sequential growth ansatz like ADAPT-VQE<sup>35</sup> where the operators are chosen based on the energy gradients with respect to individual parameters from an operator pool. COMPASS, on the other hand, is a dynamically expandable ansatz construction protocol where no such energy gradient needs to be computed to select the operators; rather, one selects the "best" set of parameters through energy optimization of one and two-parameter energy functionals in parallel quantum architecture. The tailoring protocol automatically ensures to include the most significant cluster amplitudes according to energetically optimal ordering. Appropriate scatterers are immediately allowed to act upon once an entangled state is generated through the action of cluster operators on the Hartree Fock determinant. This has shown to create a significantly compact and accurate wavefunction ansatz while excitations of arbitrarily high rank can be captured through implicit commutativity between various class of operators. The COMPASS protocol tailors the ansatz depending on the system and its associated electronic complexity under consideration, while keeping the parameter count to the minimum. The compact representation of the wavefunction makes it a desirable candidate towards its realization on a NISQ platform.

One major advantage of COMPASS is its ability to build the wavefunction ansatz in a parallel architecture, making the ansatz construction significantly less impacted by the noisy environment. The accuracy is largely controlled by the two tuneable parameters. Even with somewhat conservative choices of these parameters, the numerical results with various complex molecular systems amply demonstrate its consistent superiority over UCCSD in terms of accuracy, gate count and the ease of implementation. With high degree of quantum parallelism towards the preparation of the ansatz and its extremely low execution gate depth towards the state preparation through the parametrized circuit, COMPASS would be an extremely desirable candidate for digital molecular simulations in near-term quantum devices.

#### V. ACKNOWLEDGEMENT:

DM thanks Prime Minister's Research Fellowship (PMRF), Government of India for his research fellowship. SH thanks Council of Scientific and Industrial Research (CSIR), Government of India, and DH thanks Industrial Research and Consultancy Center (IRCC), IIT Bombay for their research fellowships.

<sup>1</sup>S. McArdle, S. Endo, A. Aspuru-Guzik, S. C. Benjamin, and X. Yuan, "Quantum computational chemistry," *Rev. Mod. Phys.* **92**, 015003 (2020).

<sup>2</sup>G. Ortiz, J. E. Gubernatis, E. Knill, and R. Laflamme, "Quantum algorithms for fermionic simulations," *Phys. Rev. A* **64**, 022319 (2001).

<sup>3</sup>J. Tilly, H. Chen, S. Cao, D. Picozzi, K. Setia, Y. Li, E. Grant, L. Wossnig, I. Rungger, G. H. Booth, and J. Tennyson, "The variational quantum eigensolver: A review of methods and best practices," *Physics Reports* **986**, 1–128 (2022).

<sup>4</sup>D. S. Abrams and S. Lloyd, "Simulation of many-body fermi systems on a universal quantum computer," *Phys. Rev. Lett.* **79**, 2586–2589 (1997).



- <sup>5</sup>D. S. Abrams and S. Lloyd, "Quantum algorithm providing exponential speed increase for finding eigenvalues and eigenvectors," *Phys. Rev. Lett.* **83**, 5162–5165 (1999).
- <sup>6</sup>D. Halder, V. S. Prasanna, V. Agarwal, and R. Maitra, "Iterative quantum phase estimation with variationally prepared reference state," *International Journal of Quantum Chemistry* **123**, e27021 (2023), <https://onlinelibrary.wiley.com/doi/pdf/10.1002/qua.27021>.
- <sup>7</sup>H. Wang, S. Kais, A. Aspuru-Guzik, and M. R. Hoffmann, "Quantum algorithm for obtaining the energy spectrum of molecular systems," *Phys. Chem. Chem. Phys.* **10**, 5388–5393 (2008).
- <sup>8</sup>A. Aspuru-Guzik, A. D. Dutoi, P. J. Love, and M. Head-Gordon, "Simulated quantum computation of molecular energies," *Science* **309**, 1704–1707 (2005), <https://www.science.org/doi/pdf/10.1126/science.1113479>.
- <sup>9</sup>A. Peruzzo, J. McClean, P. Shadbolt, M.-H. Yung, X.-Q. Zhou, P. J. Love, A. Aspuru-Guzik, and J. L. O'Brien, "A variational eigenvalue solver on a photonic quantum processor," *Nature Communications* **5** (2014), 10.1038/ncomms5213.
- <sup>10</sup>J. I. Colless, V. V. Ramasesh, D. Dahlen, M. S. Blok, M. E. Kimchi-Schwartz, J. R. McClean, J. Carter, W. A. de Jong, and I. Siddiqi, "Computation of molecular spectra on a quantum processor with an error-resilient algorithm," *Phys. Rev. X* **8**, 011021 (2018).
- <sup>11</sup>C. Hempel, C. Maier, J. Romero, J. McClean, T. Monz, H. Shen, P. Jurcevic, B. P. Lanyon, P. Love, R. Babbush, A. Aspuru-Guzik, R. Blatt, and C. F. Roos, "Quantum chemistry calculations on a trapped-ion quantum simulator," *Phys. Rev. X* **8**, 031022 (2018).
- <sup>12</sup>M. Metcalf, N. P. Bauman, K. Kowalski, and W. A. de Jong, "Resource-efficient chemistry on quantum computers with the variational quantum eigensolver and the double unitary coupled-cluster approach," *Journal of Chemical Theory and Computation* **16**, 6165–6175 (2020), pMID: 32915568, <https://doi.org/10.1021/acs.jctc.0c00421>.
- <sup>13</sup>K. Sugisaki, T. Kato, Y. Minato, K. Okuwaki, and Y. Mochizuki, "Variational quantum eigensolver simulations with the multireference unitary coupled cluster ansatz: a case study of the c2v quasi-reaction pathway of beryllium insertion into a h2 molecule," *Phys. Chem. Chem. Phys.* **24**, 8439–8452 (2022).
- <sup>14</sup>Y. Shen, X. Zhang, S. Zhang, J.-N. Zhang, M.-H. Yung, and K. Kim, "Quantum implementation of the unitary coupled cluster for simulating molecular electronic structure," *Physical Review A* **95** (2017), 10.1103/physreva.95.020501.
- <sup>15</sup>J. Romero, R. Babbush, J. R. McClean, C. Hempel, P. J. Love, and A. Aspuru-Guzik, "Strategies for quantum computing molecular energies using the unitary coupled cluster ansatz," *Quantum Science and Technology* **4**, 014008 (2018).
- <sup>16</sup>F. A. Evangelista, G. K.-L. Chan, and G. E. Scuseria, "Exact parameterization of fermionic wave functions via unitary coupled cluster theory," *The Journal of Chemical Physics* **151**, 244112 (2019), <https://doi.org/10.1063/1.5133059>.
- <sup>17</sup>I. O. Sokolov, P. K. Barkoutsos, P. J. Ollitrault, D. Greenberg, J. Rice, M. Pistoia, and I. Tavernelli, "Quantum orbital-optimized unitary coupled cluster methods in the strongly correlated regime: Can quantum algorithms outperform their classical equivalents?" *The Journal of Chemical Physics* **152**, 124107 (2020), <https://doi.org/10.1063/1.5141835>.
- <sup>18</sup>A. Anand, P. Schleich, S. Alperin-Lea, P. W. K. Jensen, S. Sim, M. Díaz-Tinoco, J. S. Kottmann, M. Degroote, A. F. Izmaylov, and A. Aspuru-Guzik, "A quantum computing view on unitary coupled cluster theory," *Chem. Soc. Rev.* **51**, 1659–1684 (2022).
- <sup>19</sup>H. Nakatsuji, "Equation for the direct determination of the density matrix," *Phys. Rev. A* **14**, 41–50 (1976).
- <sup>20</sup>M. Nooijen, "Can the eigenstates of a many-body hamiltonian be represented exactly using a general two-body cluster expansion?" *Phys. Rev. Lett.* **84**, 2108–2111 (2000).
- <sup>21</sup>J. Lee, W. J. Huggins, M. Head-Gordon, and K. B. Whaley, "Generalized unitary coupled cluster wave functions for quantum computation," *Journal of Chemical Theory and Computation* **15**, 311–324 (2018).
- <sup>22</sup>D. Halder, V. S. Prasanna, and R. Maitra, "Dual exponential coupled cluster theory: Unitary adaptation, implementation in the variational quantum eigensolver framework and pilot applications," *The Journal of Chemical Physics* **157**, 174117 (2022), <https://doi.org/10.1063/5.0114688>.
- <sup>23</sup>R. Maitra, Y. Akinaga, and T. Nakajima, "A coupled cluster theory with iterative inclusion of triple excitations and associated equation of motion formulation for excitation energy and ionization potential," *The Journal of Chemical Physics* **147**, 074103 (2017), <https://doi.org/10.1063/1.4985916>.
- <sup>24</sup>S. Tribedi, A. Chakraborty, and R. Maitra, "Formulation of a dressed coupled-cluster method with implicit triple excitations and benchmark application to hydrogen-bonded systems," *Journal of Chemical Theory and Computation* **16**, 6317–6328 (2020), pMID: 32794747, <https://doi.org/10.1021/acs.jctc.0c00736>.
- <sup>25</sup>A. Das and B. Chakrabarti, "Quantum annealing and related optimization methods," *Quantum Annealing and Related Optimization Methods*, Edited by A. Das and B.K. Chakrabarti. 2005 XIV, 378 p. 124 illus. Also available online. ISBN 3-540-27987-3. Berlin: Springer, 2005. (2005).
- <sup>26</sup>Y. Fan, C. Cao, X. Xu, Z. Li, D. Lv, and M.-H. Yung, "Circuit-depth reduction of unitary-coupled-cluster ansatz by energy sorting," (2021).
- <sup>27</sup>H. Abraham *et al.*, "Qiskit: An open-source framework for quantum computing," (2021).
- <sup>28</sup>Q. Sun, T. C. Berkelbach, N. S. Blunt, G. H. Booth, S. Guo, Z. Li, J. Liu, J. D. McClain, E. R. Sayfutyarova, S. Sharma, S. Wouters, and G. K.-L. Chan, "Pyscf: the python-based simulations of chemistry framework," *WIREs Computational Molecular Science* **8**, e1340 (2018), <https://wires.onlinelibrary.wiley.com/doi/pdf/10.1002/wcms.1340>.
- <sup>29</sup>W. J. Hehre, R. F. Stewart, and J. A. Pople, "Self-consistent molecular-orbital methods. i. use of gaussian expansions of slater-type atomic orbitals," *The Journal of Chemical Physics* **51**, 2657–2664 (1969), <https://doi.org/10.1063/1.1672392>.
- <sup>30</sup>J. T. Seeley, M. J. Richard, and P. J. Love, "The bravyi-kitaev transformation for quantum computation of electronic structure," *The Journal of Chemical Physics* **137**, 224109 (2012), <https://doi.org/10.1063/1.4768229>.
- <sup>31</sup>J. L. Morales, "A numerical study of limited memory bfgs methods," *Applied Mathematics Letters* **15**, 481–487 (2002).
- <sup>32</sup>R. H. Byrd, P. Lu, J. Nocedal, and C. Zhu, "A limited memory algorithm for bound constrained optimization," *SIAM Journal on Scientific Computing* **16**, 1190–1208 (1995), <https://doi.org/10.1137/0916069>.
- <sup>33</sup>O. R. Meitei, B. T. Gard, G. S. Barron, D. P. Pappas, S. E. Economou, E. Barnes, and N. J. Mayhall, "Gate-free state preparation for fast variational quantum eigensolver simulations," *npj Quantum Information* **7**, 155 (2021).
- <sup>34</sup>N. H. Stair and F. A. Evangelista, "Simulating many-body systems with a projective quantum eigensolver," *PRX Quantum* **2**, 030301 (2021).
- <sup>35</sup>H. R. Grimsley, S. E. Economou, E. Barnes, and N. J. Mayhall, "An adaptive variational algorithm for exact molecular simulations on a quantum computer," *Nature Communications* **10** (2019), 10.1038/s41467-019-10988-2.